

‘Phase diagram’ of interfacial instabilities in a two-layer Couette flow and mechanism of the long-wave instability

By FRANÇOIS CHARRU¹ AND E. JOHN HINCH²

¹ Institut de Mécanique des Fluides de Toulouse, 2, allée du Professeur C. Soula,
31400 Toulouse, France

² Department of Applied Mathematics and Theoretical Physics, University of Cambridge,
Silver Street, Cambridge CB3 9EW, UK

(Received 14 January 1998 and in revised form 16 February 2000)

A unified view is given of the instabilities that may develop in two-layer Couette flows, as a ‘phase diagram’ in the parameter space. This view is obtained from a preliminary study of the single-fluid Couette flow over a wavy bottom, which reveals three flow regimes for the disturbances created at the bottom, each regime being characterized by a typical penetration depth of the vorticity disturbances and an effective Reynolds number. It appears that the two-layer flow exhibits the same flow regimes for the disturbances induced by the perturbed interface, and that each type of instability can be associated with a flow regime. Typical curves giving the growth rate versus wavenumber are deduced from this analysis, and favourably compared with the existing literature. In the second part of this study, we propose a mechanism for the long wavelength instability, and provide simple estimates of the wave velocity and growth rate, for channel flows and for semi-bounded flows. In particular, an explanation is given for the ‘thin-layer effect’, which is typical of multi-layer flows such as pressure driven flows or gravity driven flows, and according to which the flow is stable if the thinner layer is the less viscous, and unstable otherwise.

1. Introduction

Interfacial instabilities in multi-layer flows have received much attention in the recent literature, for their importance in engineering processes, such as coating, polymer extrusion, oil transportation, as well as for their basic scientific significance. Three fundamental systems have been studied: gravity-driven flows such as multi-layer films on an inclined plane (Kliakhandler & Sivashinsky 1997), pressure-driven flows such as core-annular (Joseph *et al.* 1997) and plane Poiseuille flows (Laure *et al.* 1997), and shear-driven flows such as plane Couette flow. This paper is concerned with the linear stability of the latter flow of two superposed layers of immiscible fluids (figure 1). Indeed, despite the numerous papers already devoted to the subject, and although the problem is governed by the well-established Orr–Sommerfeld equation and boundary conditions, several questions remain unanswered.

Linear stability analyses have identified three types of instability. Two of them, a long-wavelength instability (Yih 1967; Hooper 1985) and a short-wavelength instability (Hooper & Boyd 1983), are low-Reynolds-number instabilities and arise from an ‘interfacial mode’. This mode comes from the jump at the interface in the slope of the

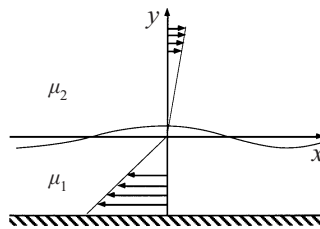


FIGURE 1. Two-layer Couette flow.

velocity profile caused by the viscosity difference, and is neutral for equal viscosity. The mechanism for the short-wave instability has been given by Hinch (1984): at the perturbed interface, the base flow velocities are discontinuous (figure 1), and velocity disturbances must develop to satisfy continuity. The resulting vorticity disturbances are in-phase with the deformed interface, but small out-of-phase components arise from advection by the base flow. The flow induced by these out-of-phase vorticity disturbances is such that the initial perturbation of the interface amplifies, at least for equal densities, corresponding to instability. The long-wave instability is linked to the presence of a wall close to the interface. Typically, when the thin layer is the less viscous, the flow is stable, and it is unstable otherwise. This ‘thin-layer effect’ is not specific to the two-layer Couette flow and also appears in multi-layer liquid films flowing down an inclined plane (Wang, Seaborg & Lin 1978) and in core-annular flows (Joseph *et al.* 1997). Experimental evidence of this instability has been presented (Barthelet, Charru & Fabre 1995; Sangalli *et al.* 1995; Charru & Barthelet 1999), but it has received no physical explanation.

Finally, the third type of instability arises from a ‘wall mode’ (Hooper & Boyd 1987), and corresponds to the classical instability of shear flows. It typically occurs at high shear rates, with a wavelength of the order of the thickness of the fluid layers (Renardy 1985).

However, it is not clear whether the above picture is complete, and the domains of existence of the above instabilities in the parameter space remain blurred. Indeed, the problem depends on six dimensionless parameters, including surface tension and gravity effects; many asymptotic expansions have been performed, as well as numerical studies, but the numerous lengthscales used to compute and discuss the results do not facilitate their comparison. As a result, it feels like having the pieces of a puzzle, whose global picture remains unknown. From the point of view of experimentalists, it is difficult to guess from the existing literature, for given flow conditions, what is the critical flow rate or pressure gradient, and the fastest growing mode.

The purpose of this paper is to clear up the above points, and to propose a unified and more physical view of the instabilities that may arise in two-layer Couette flows. A clear picture of the lengthscales involved in multi-layer flows is gained from the much simpler problem of single-fluid Couette flow over a wavy bottom (§2), which depends on two dimensionless lengths only, the layer thickness α and a viscous lengthscale β . This problem reveals three different flow regimes, each characterized by the magnitude of inertia and penetration depth of the vorticity disturbances created at the wavy bottom. Each regime lies in a particular region of the parameter space (α - β), or ‘phase diagram’. Then, coming back to the two-layer Couette flow, we analyse the existing literature with a unified set of scales, and show that the two-layer flow exhibits the same flow regimes as the single-fluid flow, and that each instability can be associated with one of these flow regimes (§3). The second part of this work

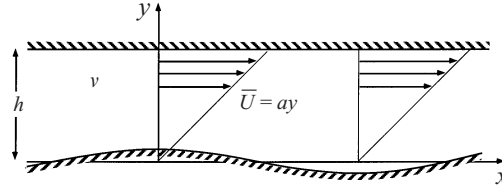


FIGURE 2. One-fluid Couette flow over a wavy bottom.

is devoted to the mechanism of the long-wave instability (§4). Simple estimates of the wave velocity and growth rate are provided, and an explanation for the ‘thin-layer effect’ is given. Surface tension and gravity effects are considered elsewhere (Albert & Charru 2000) and are ignored throughout this paper. Finally, note that the consideration of two-dimensional disturbances is justified by the fact that Squire’s theorem holds for two-layered flows (Hesla, Pranckh & Preziosi 1986), as long as marginal stability conditions are studied.

2. Couette flow over a wavy bottom

Consider the Couette flow of a fluid layer with kinematic viscosity ν and thickness h , over a wavy bottom $\hat{\eta}^{\text{dim}} \cos kx$, where superscript dim indicates dimensional (figure 2). The aim of this section is (i) to find how far the disturbances induced by the wavy bottom penetrate into the fluid, i.e. their ‘penetration depth’ δ , and (ii) to estimate inertial effects, i.e. the effective Reynolds number Re_{eff} .

2.1. The linearized problem

The velocity $\mathbf{u} = (U, V)$ and the pressure P are considered as the superposition of a base flow $\bar{U} = ay$, $\bar{V} = 0$, $\bar{P} = 0$, corresponding to a flat bottom, and stationary disturbances u, v, p created by the wavy bottom. Choosing the inverse wavenumber k^{-1} as the unit length, and the inverse shear rate a^{-1} as the unit time, the problem depends on two dimensionless parameters: the thickness α of the fluid layer and the viscous length β :

$$\alpha = kh, \quad \beta = \left(\frac{k^2 \nu}{a} \right)^{1/3}. \quad (1a)$$

The explanation for the power $\frac{1}{3}$ in the definition of β will appear below. For convenience, we also define a ‘shear Reynolds number’ Re , which is a dimensionless measure of the shear rate:

$$Re := \frac{ah^2}{\nu} = \frac{\alpha^2}{\beta^3}. \quad (1b)$$

Taking into account the symmetry $x \rightarrow x + 2\pi$ of the problem, a stationary solution for the disturbances is searched for as:

$$(u, v, p) = \frac{1}{2}((\hat{u}(y), \hat{v}(y), \hat{p}(y))e^{ix} + \text{c.c.})$$

where c.c. means complex conjugate. For small slope waves ($\hat{\eta} := k\hat{\eta}^{\text{dim}} \ll 1$), the solution can be searched for from the linearized mass and momentum conservation equations:

$$i\hat{u} + \partial_y \hat{v} = 0, \quad (2)$$

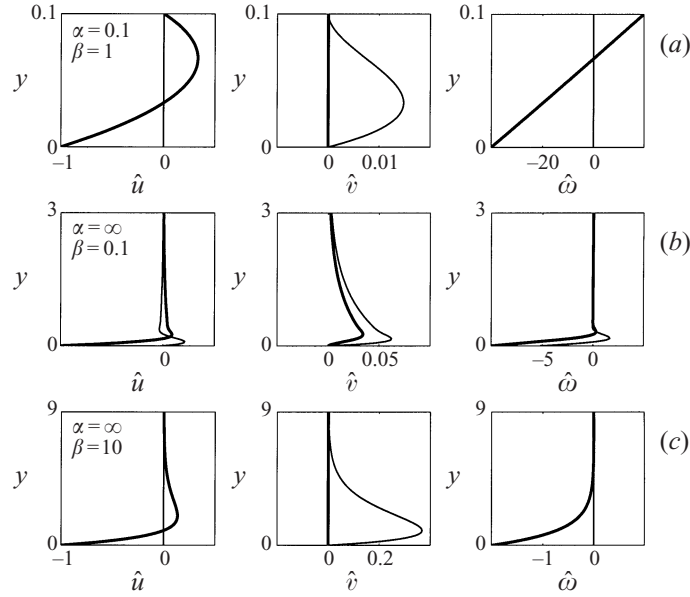


FIGURE 3. Amplitudes of the disturbances. From left to right: \hat{u} , \hat{v} and $\hat{\omega}$; from top to bottom: $\alpha = 0.1, \beta = 1$; $\alpha = \infty, \beta = 0.1$; $\alpha = \infty, \beta = 10$. Bold line: real part (component in phase with the bottom), plain line: imaginary part (component with phase leading by 90° that of the bottom).

$$iy\hat{u} + \hat{v} = -i\hat{p} + \beta^3(-\hat{u} + \partial_y^2\hat{u}), \quad (3a)$$

$$iy\hat{v} = -i\partial_y\hat{p} + \beta^3(-\hat{v} + \partial_y^2\hat{v}), \quad (3b)$$

and the no-slip boundary conditions at the walls:

$$\hat{u}(0) = -\hat{\eta}, \quad \hat{v}(0) = 0, \quad (4a)$$

$$\hat{u}(\alpha) = 0, \quad \hat{v}(\alpha) = 0. \quad (4b)$$

Since the problem to be solved is linear, we impose the normalization condition $\hat{\eta} = 1$.

2.2. Exact solution for the linearized problem and 'phase diagram'

The exact solution of (2), (3), and (4) can be obtained from the vorticity equation:

$$iy\hat{\omega} = \beta^3(-\hat{\omega} + \partial_y^2\hat{\omega}), \quad (5)$$

which can be put in the standard Airy equation $\partial_z^2\hat{\omega} - z\hat{\omega} = 0$ through the transformation $z = e^{i\pi/6}(y - i\beta^3)/\beta$. The solution of (5) is the linear combination of the Airy functions $\text{Ai}(z)$ and $\text{Bi}(z)$:

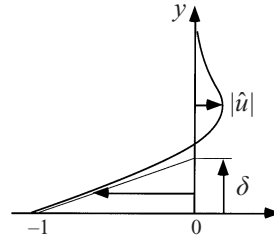
$$\hat{\omega} = C_1\text{Ai}(z) + C_2\text{Bi}(z). \quad (6)$$

Then, the streamfunction ψ can be obtained from the equation $\partial_y^2\hat{\psi} - \hat{\psi} = -\hat{\omega}$, whose solution is:

$$\hat{\psi}(y) = \frac{1}{2} \left\{ e^{-y} \int_0^y e^Y \hat{\omega}(Y) dY + e^y \int_y^\alpha e^{-Y} \hat{\omega}(Y) dY \right\} + C_3 e^{-y} + C_4 e^y. \quad (7)$$

The constants C_1, C_2, C_3 and C_4 can be determined from the boundary conditions (4) on $\hat{u} = \partial_y\hat{\psi}$ and $\hat{v} = -i\hat{\psi}$: they are given in Appendix A.

A first idea of the penetration depth δ of the disturbances can be gained from figure 3, which displays the real and imaginary parts of the amplitude of velocity and


 FIGURE 4. Definition of the penetration depth δ .

vorticity disturbances for three typical cases. Figure 3(a) shows that for $\alpha = 0.1$ and $\beta = 1$, disturbances diffuse up to the upper wall. Thus, the penetration depth δ is the layer thickness α , and transverse gradients ∂_y are $O(1/\alpha)$. As proved below, these features are encountered more generally for $\alpha < 1$ and $\beta > \alpha$, and this type of flow will be referred to as the ‘shallow viscous regime’. Figure 3(b) shows that for $\alpha = \infty$ and $\beta = 0.1$, the penetration depth divides into two parts: a thin layer of rotational flow with strong gradients close to the interface, surrounded by a region of potential flow decaying exponentially. These features are encountered more generally for $\alpha > 1$ and $\beta < 1$, and this type of flow will be referred to as the ‘inviscid regime’. Finally, figure 3(c) shows that for $\alpha = \infty$ and $\beta = 10$, the thickness of the penetration depth is $O(1)$, i.e. roughly equal to one wavelength. This remains true more generally for $\alpha > 1$ and $\beta > 1$, and this type of flow will be referred to as the ‘deep viscous regime’.

A first idea of the importance of inertial effects can also be gained from figure 3. Indeed, inertial effects are expected to shift the disturbances created by the wavy bottom, so that the magnitude of inertial effects can be measured by the imaginary part of the disturbances. For the shallow viscous regime and the deep viscous regime, the velocity u and the vorticity ω are essentially in phase with the interface: this corresponds to small inertial effects. The phase of the velocity v leads by 90° the phase of the bottom, and disturbances form cells rotating clockwise above the peaks and anticlockwise above the troughs. For the inviscid regime, the real and imaginary components have same order of magnitude: the rotating cells formed by the disturbances are shifted downstream by significant inertial effects.

The above remarks can be made more precise by introducing the following definitions of the penetration depth of vorticity disturbances (figure 4) and of the effective Reynolds number Re_{eff} measuring inertial effects:

$$\delta := |\partial_y \hat{u}(0)|^{-1} = |\hat{\omega}(0)|^{-1}, \quad (8a)$$

$$Re_{eff} := \frac{\hat{\omega}_i(0)}{\hat{\omega}_r(0)}. \quad (8b)$$

Figure 5 displays the penetration depth δ and the effective Reynolds Re_{eff} number versus β , for several α . Figures 5(a) and 5(b) show that for $\alpha > 1$, an asymptotic regime is reached from $\alpha = 5$. In this regime, $\delta \sim \beta$ and $Re_{eff} \sim 1$ for $\beta < 1$, and $\delta \sim 1$ and $Re_{eff} \sim \beta^{-3}$ for $\beta > 1$. Figures 5(c) and 5(d) show that for $\alpha < 2$, an asymptotic regime is nearly reached from $\alpha = 1$. In this regime, $\delta \sim \beta$ and $Re_{eff} \sim 1$ for $\beta < \alpha$, and $\delta \sim \alpha$ and $Re_{eff} \sim (\alpha/\beta)^3 = \alpha Re$ for $\beta > \alpha$. Note that the transitions between the asymptotic domains are sharp and occur over less than one decade. These results are summarized in the $(\log \beta, \log \alpha)$ plane (figure 6), which can be considered as the ‘phase diagram’ of the Couette flow over a wavy bottom. This plane is divided into three regions, corresponding to the shallow viscous regime, the inviscid regime, and

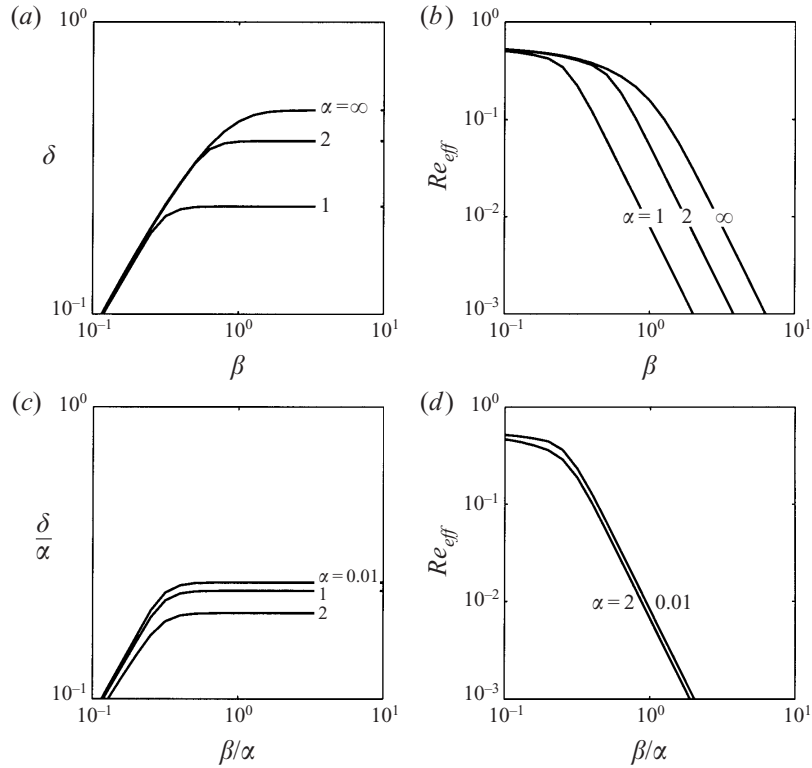


FIGURE 5. (a) Penetration depth δ and (b) effective Reynolds number Re_{eff} versus β for $\alpha \geq 1$. (c) Penetration depth δ/α and (d) effective Reynolds number Re_{eff} versus β/α for $\alpha \leq 1$.

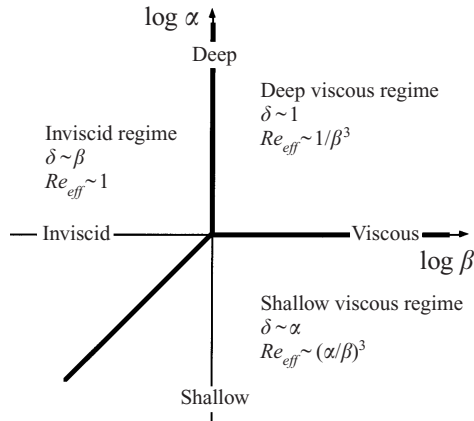


FIGURE 6. 'Phase diagram' of the Couette flow over a wavy boundary.

the deep viscous regime. Each flow regime is defined by its penetration depth δ and effective Reynolds number Re_{eff} . Finally, note that in all regions δ and Re_{eff} satisfy:

$$\delta = \min(1, \alpha, \beta), \tag{9a}$$

$$Re_{eff} = \min(1, 1/\beta^3, (\alpha/\beta)^3). \tag{9b}$$

The fact that the penetration depth of the inviscid regime scales as β can be understood from the vorticity equation (5). Indeed, when the penetration depth is much thinner than the wavelength, transverse gradients ∂_y dominate and (5) reduces to $i\gamma\hat{\omega} = \beta^3\partial_y^2\hat{\omega}$. Setting $y \sim \delta$ and $\partial_y \sim 1/\delta$ in the above equation leads to $\delta \sim \beta$, which justifies the definition (1a) of β .

2.3. Asymptotic solutions in the three regimes

All the above results can be confirmed from asymptotic expansions. In the shallow viscous regime ($\alpha \ll 1$ and $\beta > \alpha$), the asymptotic solution of (3) and (4) can be found by rescaling the thickness of the layer to unity by the change of variable $Y = y/\alpha$, so that the gradients appearing in (3) are $O(1)$. Expanding the disturbances in powers of α and assuming $Re = O(1)$, the solution for the first two orders is found to be:

$$\hat{u} = (Y - 1)(1 - 3Y) + i\alpha\frac{Re}{30}Y(1 - Y)^2(1 - Y - 3Y^2) + O(\alpha^2),$$

$$\hat{v} = i\alpha Y(Y - 1)^2 + \alpha^2\frac{Re}{60}Y^2(1 - Y)^3(1 + Y) + O(\alpha^3),$$

$$\hat{p} = i\frac{6}{Re} - \frac{\alpha}{5} + O(\alpha^2).$$

Dominant terms correspond to Stokes flow, whereas correction terms take into account small inertial effects. (Note that the amplitude of the dimensional pressure is $\hat{p} \rho(a/k)^2(k\hat{\eta}^{\text{dim}}) = 6(\hat{\eta}^{\text{dim}}/h)^2\mu a/k\hat{\eta}^{\text{dim}}$: for fixed $\hat{\eta}^{\text{dim}}/h$, it diverges for small wave slope as $1/(k\hat{\eta}^{\text{dim}})$, which corresponds to the classical result for the lubrication pressure (Batchelor 1967).) Thus, the vorticity at the wavy bottom is:

$$\hat{\omega}(0) = -\frac{4}{\alpha} - i\frac{Re}{30} + O(\alpha) \quad (10)$$

from which the penetration depth and the effective Reynolds number are obtained:

$$\delta = \frac{1}{4}\alpha + O(\alpha^2) \quad (11a)$$

$$Re_{\text{eff}} = \frac{\alpha Re}{120} + O(\alpha^2). \quad (11b)$$

These results agree with the exact results displayed in figure 5: the penetration depth is $O(\alpha)$ and inertial effects are $O(\alpha Re)$.

In the inviscid regime ($\alpha > \beta$ and $\beta \ll 1$), the upper wall is expected to have no effect, and the thickness α , which appears in the no-slip conditions at the upper wall only, disappears from the problem. Transverse gradients are expected to be $O(1/\beta)$, and are rescaled to $O(1)$ by the change of variable $Y = y/\beta$. Expanding the disturbances in powers of β , the solution at dominant order for \hat{u} is found to be:

$$\hat{u} = -\frac{\int_Y^\infty \text{Ai}(e^{i\pi/6}Y) dY}{\int_0^\infty \text{Ai}(e^{i\pi/6}Y) dY} + O(\beta) \quad \text{with} \quad \int_0^\infty \text{Ai}(e^{i\pi/6}Y) dY \approx 0.336 e^{-i\pi/6},$$

with similar expressions involving integrals of Airy functions for \hat{v} and \hat{p} . Thus, the

vorticity at the wavy bottom is:

$$\hat{\omega}(0) = -\frac{1}{\beta} \frac{\text{Ai}(0)}{\int_0^\infty \text{Ai}(e^{i\pi/6} Y) dY} + O(\beta^0) \approx -\frac{1.06}{\beta} e^{i\pi/6} + O(\beta^0), \quad (12)$$

and the penetration depth and the effective Reynolds number are:

$$\delta \approx \frac{\beta}{1.06} + O(\beta^2), \quad (13a)$$

$$Re_{eff} \approx 0.577 + O(\beta). \quad (13b)$$

These results agree with the exact results shown in figures 3 and 4: the penetration depth is $O(\beta)$ and inertial effects are found from dominant order and are $O(1)$.

Finally, in the deep viscous regime ($\alpha \gg 1$ and $\beta \gg 1$), the upper wall is expected to have no effect, and the thickness α disappears from the problem as in the inviscid regime. Transverse gradients are expected to be $O(1)$. Expanding the disturbances in powers of $1/\beta^3$, the solution of (3) and (4) for the first two orders is found to be:

$$\hat{u} = (y-1)e^{-y} + \frac{i}{12\beta^3} y(6-y)e^{-y} + O(1/\beta^6),$$

$$\hat{v} = iye^{-y} + \frac{1}{12\beta^3} y^2(3+y)e^{-y} + O(1/\beta^6),$$

$$\hat{p} = 2i\beta^3 e^{-y} - \frac{1}{2}(2+y+y^2)e^{-y} + O(1/\beta^3).$$

As for the shallow viscous regime, dominant terms correspond to Stokes flow, and correction terms account for small inertial effects. (Again, \hat{p} scales as $\beta^3 \gg 1$ which corresponds to the lubrication pressure.) Thus, the vorticity at the wavy bottom is:

$$\hat{\omega}(0) = -2 - \frac{1}{2}i\frac{1}{\beta^3} + O\left(\frac{1}{\beta^6}\right) \quad (14)$$

and the penetration depth and the effective Reynolds number are:

$$\delta = \frac{1}{2} + O\left(\frac{1}{\beta^3}\right), \quad (15a)$$

$$Re_{eff} = \frac{1}{4\beta^3} + O\left(\frac{1}{\beta^6}\right). \quad (15b)$$

Again, these results agree with the exact results shown in figures 3 and 4: the penetration depth is $O(1)$ and inertial effects are $O(\beta^{-3})$.

3. Two-layer Couette flow

The aim of this section is to provide a unified view of the stability results previously obtained for the two-layer Couette flow, from the construction of phase diagrams similar to that brought out in the previous section.

3.1. The linearized problem

Guided by the single-fluid problem discussed in the previous section, we define for each fluid a dimensionless thickness and a dimensionless viscous length:

$$\alpha_j := kh_j, \quad \beta_j = \left(\frac{k^2 \nu_j}{a_j} \right)^{1/3}. \quad (16a)$$

Together with the viscosity ratio m or the density ratio r :

$$m := \frac{\mu_2}{\mu_1}, \quad r := \frac{\rho_2}{\rho_1}, \quad (16b)$$

the above lengthscales completely define the problem, when gravity and surface tension are ignored. The six parameters (16) are not independent: continuity of shear stress at the interface for the base flow, $\mu_1 a_1 = \mu_2 a_2$, gives:

$$\frac{\beta_2^3}{\beta_1^3} = \frac{m^2}{r}. \quad (17)$$

For convenience, we also define the ‘shear Reynolds number’ of the lower fluid as:

$$Re := \frac{a_1 h_1^2}{\nu_1} = \frac{\alpha_1^2}{\beta_1^3}. \quad (18)$$

Taking k^{-1} as the unit length and a_1^{-1} as the unit time, the base flow is given by $\bar{U}_1 = y$, $\bar{U}_2 = y/m$, and the linearized conservation equations for the amplitudes of the normal modes $\exp\{i(x - ct)\}$ are:

$$i\hat{u}_j + \partial_y \hat{v}_j = 0 \quad (j = 1, 2), \quad (19a)$$

$$i(y/m_j - c)\hat{u}_j + \hat{v}_j/m_j = -\frac{i\hat{p}_j}{r_j} + \frac{\beta_j^3}{m_j}(-\hat{u}_j + \partial_{yy}\hat{u}_j) \quad (j = 1, 2), \quad (19b)$$

$$i(y/m_j - c)\hat{v}_j = -\frac{\partial_y \hat{p}_j}{r_j} + \frac{\beta_j^3}{m_j}(-\hat{v}_j + \partial_{yy}\hat{v}_j) \quad (j = 1, 2), \quad (19c)$$

where $r_1 = 1$, $r_2 = r$, $m_1 = 1$, $m_2 = m$. The no-slip conditions at the walls are:

$$\hat{u}_1(-\alpha_1) = 0, \quad \hat{v}_1(-\alpha_1) = 0, \quad (20a)$$

$$\hat{u}_2(\alpha_2) = 0, \quad \hat{v}_2(\alpha_2) = 0, \quad (20b)$$

the linearized equations for continuity of velocity and stress at the interface $y = 0$ are:

$$\hat{\eta} + \hat{u}_1 = \frac{\hat{\eta}}{m} + \hat{u}_2, \quad (20c)$$

$$\hat{v}_1 = \hat{v}_2, \quad (20d)$$

$$\partial_y \hat{u}_1 + i\hat{v}_1 = m(\partial_y \hat{u}_2 + i\hat{v}_2), \quad (20e)$$

$$-(\hat{p}_2 - \hat{p}_1) + 2\frac{r\beta_2^3}{m}\partial_y \hat{v}_2 - 2\beta_1^3\partial_y \hat{v}_1 = 0, \quad (20f)$$

and the linearized no-mass transfer at the interface (or kinematic condition) is:

$$i\hat{\eta}c + \hat{v}_j = 0. \quad (20g)$$

Note that the equations for the single-fluid problem addressed in the previous section

Shallow viscous $\times 2$ regime (Yih 1967)	$d \gg 1$	$\frac{c^{\text{dim}}}{a_1 h_1} = \frac{2(1-m)}{d} + O(\alpha_1^2)$
		$\frac{\sigma^{\text{dim}}}{a_1} = \alpha_1^2 Re(1-m) \frac{rd^2}{60m^2} + O(\alpha_1^4)$
	$ 1-m \ll 1$	$\frac{c^{\text{dim}}}{a_1 h_1} = \frac{1-m}{4} + O(\alpha_1^2)$
	$ 1-d \ll 1$	$\frac{\sigma^{\text{dim}}}{a_1} = \alpha_1^2 Re(1-m) \frac{7(1-r)}{960} + O(\alpha_1^4)$
Deep viscous $\times 2$ regime (Hooper & Boyd 1983)		$\frac{c^{\text{dim}}}{a_1 h_1} = 0 + O(1/\beta_1^6)$
		$\frac{\sigma^{\text{dim}}}{a_1} = \frac{1}{\beta_1^3} \frac{(1-m)(r-m^2)}{2m^2(1+m)^2} + O(1/\beta_1^9)$
Inviscid $\times 2$ regime, $r = 1$ (Hooper & Boyd 1983)		$c^{\text{dim}} \sim \frac{a_1}{k} \frac{1-m}{2m}$
		$\frac{\sigma^{\text{dim}}}{a_1} \sim -2(1+m)\beta_1^3$

TABLE 1. Dimensional wave velocity c^{dim} and growth rate σ^{dim} of the interfacial mode for channel flows. Since $m = O(1)$, $d = O(1)$ and $r = O(1)$, then $\beta_1 \sim \beta_2$ and $\alpha_1 \sim \alpha_2$, and both flows are in the same regime. For the wall mode, see Appendix B.

are recovered from the above equations with lower fluid of infinite density and viscosity, after the unit time has been changed to a_2^{-1} .

Finally, extending the definitions (8) to the two-fluid flow, we define the penetration depth δ_j of the vorticity disturbances and the effective Reynolds number Re_{effj} in each fluid as:

$$\delta_j := |\partial_y \hat{u}_j(0)|^{-1} = |\hat{\omega}_j(0)|^{-1} \quad (j = 1, 2), \quad (21a)$$

$$Re_{effj} := \frac{\hat{\omega}_j(0)}{\hat{\omega}_j(0)} \quad (j = 1, 2), \quad (21b)$$

where $\hat{\omega}_{jr}$ and $\hat{\omega}_{ji}$ are the real part and imaginary part of the vorticity disturbance in fluid j , respectively.

3.2. 'Phase diagram' for channel flows (finite α_1 and α_2)

Two different cases have been considered in the literature. The first case corresponds to channel flows, i.e. finite α_1 and α_2 ($d = h_2/h_1 = \alpha_2/\alpha_1 = O(1)$), and the second case, to semi-bounded flows, i.e. finite α_1 and $\alpha_2 = \infty$ ($d = \infty$). The asymptotic results for the wave velocity and growth rate are summarized in this subsection for channel flows (table 1), and in the next subsection for semi-bounded flows (table 2). All studies assume fluid properties to be of the same order of magnitude, i.e. $m = O(1)$ and $r = O(1)$, so that $\beta_2 \sim \beta_1$ (for air over water, $\beta_a/\beta_w = 0.6$, and for viscous oil over water with $\mu_o/\mu_w = 30$, $\beta_o/\beta_w \approx 10$).

The stability of channel flows against long-wavelength disturbances has been studied by Yih (1967), who performed a long-wave expansion similar to that performed here

in § 2.3, with:

$$\alpha_1 \ll 1, \quad Re = O(1). \tag{22}$$

The wave velocity and the growth rate have complicated the expressions given in Appendix C. Table 1 gives simpler expressions for two limits: (i) similar layers ($m \approx 1$ and $d \approx 1$), and (ii) layers with very different thickness ($d \gg 1$, or more precisely $\alpha_1 \ll \alpha_2 \ll 1$). The most important feature is that the growth rate is proportional to $\alpha_1^2 Re(1 - m)$: instability is entirely due to the viscosity difference of the layers, and arises however small the shear Reynolds number is. Finally, the penetration depth is $\delta_j \sim \alpha_j$ and the effective Reynolds number is $Re_{effj} \sim \alpha_j^3/\beta_j^3$: the flow within each layer is in the ‘shallow viscous regime’ defined in § 2 for the single-fluid Couette flow.

The stability against short-wavelength disturbances has been studied by Hooper & Boyd (1983) from a short-wave expansion similar to that performed here in § 2.5, with:

$$\beta_1^3 \gg 1, \quad \alpha_1 = \alpha_2 = \infty. \tag{23}$$

It appears that for equal density, short waves are always unstable when surface tension is ignored. The mechanism for this instability has been given by Hinch (1984) and was outlined in the introduction of this paper. Eigenfunctions decay exponentially away from the interface with penetration depth $\delta_j \sim 1$, and the effective Reynolds number is $Re_{effj} \sim 1/\beta_j^3$: the flow within each layer is in the ‘deep viscous regime’ defined in § 2. The effect of the walls (finite thicknesses) has been taken into account by Hooper (1989), assuming equal density. This study gives more accurate results in the deep viscous regime for $\alpha_1 \sim \alpha_2$ close to unity, and shows that a wall has no effect as soon as the layer thickness is greater than the wavelength ($kh_j > 6$). However, this expansion is unable to give the right growth rate and wave velocity for long waves, because the limits $\beta_1^3 \rightarrow \infty$ and $\alpha_1 \rightarrow 0$ are not interchangeable.

The third case for channel flows corresponds to:

$$\beta_1/\alpha_1 \ll 1 \quad \text{with} \quad \beta_1 \ll 1. \tag{24}$$

It has been studied by Hooper & Boyd (1983) for unbounded fluid layers ($\alpha_1 = \alpha_2 = \infty$) from an asymptotic analysis for $\beta_1 \ll 1$ of the exact dispersion relationship. All eigenmodes are found to be stable, and table 1 gives the wave velocity and growth rate of the least stable mode. The form of the eigenfunctions indicates that the penetration depth is $O(\beta_j)$ and inertial effects are $O(1)$. For bounded layers, these results are expected to remain valid as long as $\beta_1/\alpha_1 \ll 1$, and this is confirmed by numerical studies (Renardy 1985; Hooper & Boyd 1987; Albert & Charru 2000). Thus the flow within each layer is in the ‘inviscid regime’ defined in § 2.

The above discussion is synthesized on the ‘phase diagram’ (figure 7a), similar to that of the single-fluid Couette flow (figure 6). The boundaries separating the various regimes are the same for the two fluids. The scaling laws for the penetration depths δ_j and for the effective Reynolds number Re_{effj} are the same as for the single-fluid Couette flow. The growth rate is $O(\alpha_1 Re_{eff1}) = O(\alpha_2 Re_{eff2})$ in the shallow viscous regime, and is $O(Re_{eff1}) = O(Re_{eff2})$ in the deep viscous regime. In the inviscid regime, the interfacial mode is always stable and its damping rate is $O(\beta_1^3) = O(\beta_2^3)$.

3.3. ‘Phase diagram’ for semi-bounded flows (finite $\alpha_1, \alpha_2 = \infty$)

For the deep viscous and inviscid regimes discussed above, the walls play no role, so that there is no difference between channel flow and semi-bounded flow (in the deep viscous regime, the asymptotic expansion in powers of $1/\beta_1^3 \ll 1$ performed by Hooper & Boyd (1987, § 4.4) only gives more accurate results for α_1 close to unity

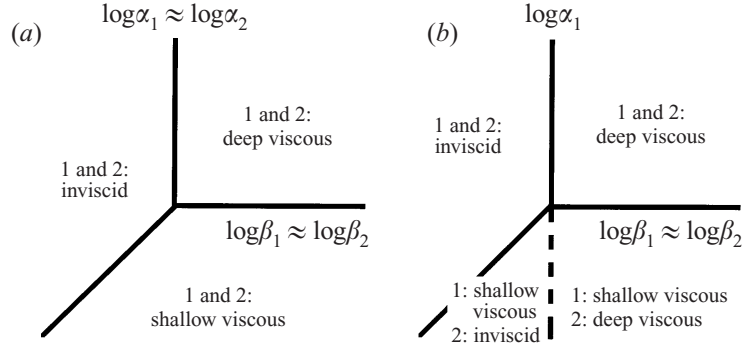


FIGURE 7. 'Phase diagram' of the two-layer Couette flow, (a) channel flow; (b) semi-bounded flow.

Shallow viscous/inviscid regime (Hooper 1985)	$\frac{c^{\text{dim}}}{a_1 h_1} = 0.46(1-m)\alpha_1^{1/3} \left(\frac{rRe}{m^2}\right)^{1/3} + O(\alpha_1^{2/3})$ $\frac{\sigma^{\text{dim}}}{a_1} = 0.27(1-m)\alpha_1^{4/3} \left(\frac{rRe}{m^2}\right)^{1/3} + O(\alpha_1^{5/3})$
Deep viscous $\times 2$ regime (Hooper & Boyd 1987)	$\frac{c^{\text{dim}}}{a_1 h_1} \sim \frac{\alpha_1(1-m)}{(\cosh \alpha_1 + m \sinh \alpha_1)^2 + \alpha_1^2(1-m^2)}$ <p>No expression available for σ^{dim}; for $\alpha_1 \rightarrow \infty$, see table 1.</p>

TABLE 2. Dimensional wave velocity c^{dim} and growth rate σ^{dim} for semi-bounded flows ($\alpha_2 = \infty$). Since $m = O(1)$ and $r = O(1)$, then $\beta_1 \sim \beta_2$. For the wall mode, see Appendix B.

(table 2)). Differences appear only when the lower fluid is in the shallow viscous regime ($\alpha_1 \ll 1$ and $\alpha_1 \ll \beta_1$). This case has been studied by Hooper (1985), matching the long-wave expansion of Yih in the lower fluid to the exact solution in the upper fluid, with:

$$\alpha_1 \ll 1, \quad \alpha_2 = \infty, \quad Re = O(1). \quad (25)$$

Waves are dispersive and the growth rate is stronger than in the channel flow case: it scales as $k^{4/3}$ rather than k^2 (table 2). The upper fluid is in the inviscid regime for $\beta_1 \sim \beta_2 \ll 1$, and in the deep viscous regime for $\beta_1 \sim \beta_2 \gg 1$. The case of fluids with similar viscosity and density was tackled by Renardy (1987) as a perturbation of the single-fluid problem. Unfortunately, no significant simplification arises from this case, and physical information seems hard to obtain from the complicated expression of the perturbed eigenvalue, unless some additional long- or short-wave limit is taken.

The above discussion is synthesized on the 'phase diagram' shown in figure 7(b). The regions for the inviscid regime and deep viscous regime are the same as for channel flows, but the former region of the shallow viscous regime is now divided into two parts, depending on whether $\beta_1 \sim \beta_2 \ll 1$ or $\beta_1 \sim \beta_2 \gg 1$. Finally, note that the penetration depth and the effective Reynolds number satisfy:

$$\delta_j = \min(1, \alpha_j, \beta_j), \quad (26a)$$

$$Re_{\text{eff}j} = \min(1, 1/\beta_j^3, (\alpha_j/\beta_j)^3). \quad (26b)$$

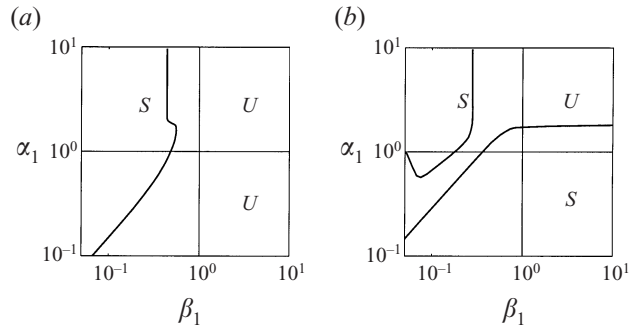


FIGURE 8. Marginal stability curves for semi-bounded Couette flow, from figures 3, 6 and 7 of Hooper & Boyd (1987). (a) $m = 0.5$, asymptotes: $\alpha/\beta = 1.47$ and $\beta = 0.438$; (b) $m = 2$, asymptotes: $\alpha/\beta = 3.11$, $\alpha = 1.8$ and $\beta = 0.276$. These curves follow the boundaries of the flow regimes defined in figure 7.

3.4. Relevance of the phase diagram from numerical results

Along with asymptotic studies, numerical studies have been performed for $\alpha_1 = O(1)$ or $Re \gg 1$ (Renardy 1985; Hooper & Boyd 1987; Albert & Charru 2000). Marginal stability curves are generally shown in the (Re, α_1) -plane or in the $(\alpha_1/\beta_1, \alpha_1)$ -plane; however, plotting these curves in the (β_1, α_1) -plane is more informative: each type of instability is clearly isolated, and the relevance of the phase diagram (figure 7) can be confirmed. As an example, figure 8 displays figures 6 and 7 of Hooper & Boyd (1987) redrawn in the (β_1, α_1) -plane. Densities are equal, so that short waves are unstable in both cases. For $m = 0.5$ (figure 8a), long waves are unstable (thin-layer effect), so that there is no marginal curve between the shallow viscous and the deep viscous regimes; the marginal stability curve follows the boundary of the inviscid regime. For $m = 2$ (figure 8b), one of the two marginal curves follows the boundary of the shallow viscous regime: long waves are stable, in agreement with the thin-layer effect; the vertical part of the second marginal curve separates the unstable deep viscous regime from the stable inviscid regime. However, for $\beta_1 \ll 1$ and $\alpha_1 = O(1)$, i.e. for strong shear Reynolds number ($Re = \alpha_1^2/\beta_1^3 \gg 1$), another unstable region appears, the nature of which is discussed below.

The small- Re eigenmodes discussed until now are clearly ‘interfacial modes’ in the sense that they exist because of the presence of the interface, and that disturbances are essentially localized in the vicinity of the interface. Another signature of an interfacial mode can be found from the kinetic energy equation, which shows that instability arises from the small difference between the rate of energy dissipation (always negative) and the net rate of work done at the interface by shear stress disturbances (Hooper & Boyd 1983; Goussis & Kelly 1988; Albert & Charru 2000). However, tracing the interfacial mode for increasing Re shows that the nature of the instability changes for high Re : the maximum of the eigenfunctions lies near the walls, and the kinetic energy equation shows that instability now arises from energy transfer from the mean flow to disturbances via the Reynolds stresses; for Couette flow, there is no crossing of the interfacial mode with a shear mode as it might occur for Poiseuille flow (Albert & Charru 2000). This mode of instability, which corresponds to the classical wall mode of single-fluid shear flows, has been studied by Hooper & Boyd (1987) from a singular perturbation method matching an inviscid solution in the bulk of each fluid to viscous boundary layers at the walls and at the interface. The solution is found as series expansions in powers of $(\alpha_1 Re)^{-1/2} = (\beta_1/\alpha_1)^{3/2}$, which

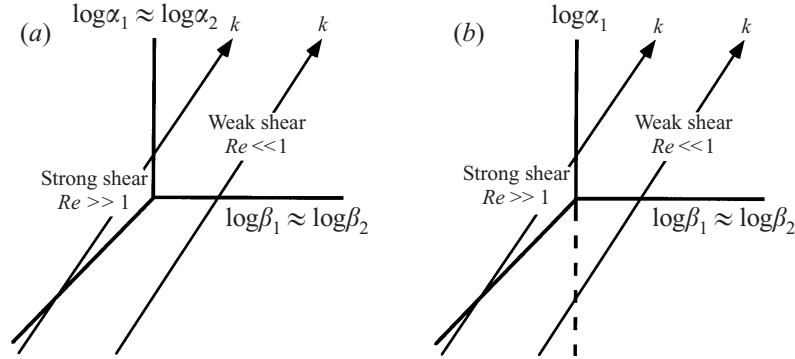


FIGURE 9. (a) channel flow; (b) semi-bounded flow. Arrows are lines of increasing k at constant shear rate (slope $\frac{3}{2}$). Left-hand line: strong shear ($Re = a_1 h_1^2 / \nu_1 = \alpha_1^2 / \beta_1^3 \gg 1$); right-hand line: weak shear ($Re \ll 1$).

is the order of magnitude of the thickness of the boundary layers. The wave velocity and growth rate are given in Appendix B for the case of equal density ($r = 1$). Note that the growth rate is of order $\beta_1^{3/2} = k(v_1/a_1)^{1/2}$ and that instability arises when the thin layer is the less viscous ($m > 1$), unlike the ‘thin-layer effect’ which holds for small Re .

3.5. The experimental point of view

From the experimental point of view, there are two important questions. (i) For given flow conditions, i.e. for given fluids and shear rate, what is the most amplified wavenumber and its growth rate? More precisely, what does the curve $\sigma(k)$ look like? (ii) How does this curve change as the shear rate changes?

For given fluid properties, constant shear rate corresponds to constant $Re := a_1 h_1^2 / \nu_1 = \alpha_1^2 / \beta_1^3$, i.e. to the oblique lines drawn in figure 9. Along one of these lines, the dimensional wavenumber varies from zero (bottom left-hand quadrant) to infinity (top right-hand corner). Increasing the shear rate shifts the line to the left. Typical curves $\sigma(k)$ can then be obtained easily. First, consider small shear rate ($Re \ll 1$). Small wavenumbers ($\alpha_1 \ll 1$) lie in the shallow viscous regime, with growth rate scaling as k^2 for channel flow and $k^{4/3}$ for semi-bounded flow; high wavenumbers ($\alpha_1 \gg 1$) lie in the deep viscous regime, with growth rate scaling as $\pm k^{-2}$. For unstable short waves, the corresponding curves $\sigma(k)$ are sketched in figure 10(a), for stable and unstable long waves. For strong shear rate ($Re \gg 1$), an intermediate region appears between the long- and short-wave regions for $\alpha_1 \in [Re^{-1}, Re^{1/2}]$, which corresponds to the stable inviscid regime. Figure 10(b) displays two typical curves $\sigma(k)$, for stable and unstable long waves. For stronger shear rate, a new wall instability, not shown on the figure, arises with $\alpha_1 = O(1)$.

4. Mechanism of the long-wave instability

Why are long waves stable if the thinner layer is less viscous, and unstable if more viscous, however small the shear Reynolds number is? The aim of this section is to provide a physical explanation for this ‘thin-layer effect’, and to understand how the presence of the walls modifies the short-wave mechanism given by Hinch (1984). The style is now changing a little to a physical argument supported by mathematical descriptions. For this purpose, dimensional quantities are used. Three

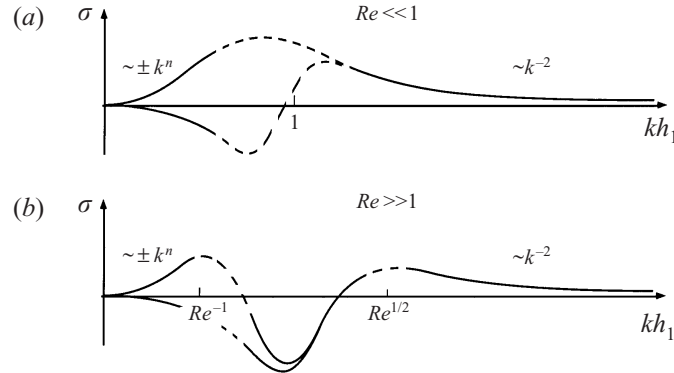


FIGURE 10. Typical curves for the growth rate σ versus wavenumber k . (a) Small shear rate ($Re \ll 1$); (b) strong shear rate ($Re \gg 1$); $n = 2$ for channel flow and $n = \frac{4}{3}$ for semi-bounded flow; the upper (lower) curve corresponds to unstable (stable) long waves.

typical situations are considered: channel flow with one layer much thinner than the other (§ 4.1), channel flow with nearly equal layer thickness (§ 4.2), and semi-bounded flow over a thin layer (§ 4.3). For each case, the estimates for the wave velocity and growth rate are compared with available asymptotic results. The shear Reynolds number Re is assumed to be small, and the viscosity and density ratios m and r are $O(1)$.

4.1. Channel flow: case of a thin layer ($\alpha_1 \ll \alpha_2 \ll 1$)

Consider a small-amplitude disturbance of the interface, $\eta = \hat{\eta} \cos k(x - ct)$ (figure 11(a)). Owing to the viscosity difference, the base velocities are not equal at the disturbed interface, and velocity disturbances must develop for the continuity of longitudinal velocity to be satisfied, according to:

$$a_1 \hat{\eta} + \hat{u}_1(0) = a_2 \hat{\eta} + \hat{u}_2(0). \quad (27)$$

When $\mu_2 > \mu_1$, the lower fluid slows down and the upper fluid speeds up, at both the peaks and troughs of the wave. Thus, the disturbance \hat{u}_1 is negative and \hat{u}_2 is positive, at least near the interface. When $\mu_2 < \mu_1$, these velocity disturbances are reversed.

For small shear Reynolds number and long waves, disturbances diffuse away from the interface up to the walls, and a linear shear flow might be expected in both fluids; but linear flows generally do not satisfy the requirements of no net flow (mass conservation) and continuity of the y -velocity at the interface, i.e.

$$\int_{-h_1}^0 \hat{u}_1 dy = -\frac{\hat{v}_1(0)}{ik} = -\frac{\hat{v}_2(0)}{ik} = \int_{h_2}^0 \hat{u}_2 dy. \quad (28)$$

Hence, pressure disturbances develop (figure 11(b)). However, the pressure driven flow is much smaller in the thin layer than in the thick layer, so that the flow in the thin layer is very close to a linear shear flow. Then, continuity of shear stress,

$$\mu_1 \partial_y \hat{u}_1(0) = \mu_2 \partial_y \hat{u}_2(0), \quad (29)$$

requires only small velocities in the thin layer. Thus, continuity of x -velocity (27) gives at the leading order:

$$U := \hat{u}_2(0) = (a_1 - a_2) \hat{\eta} = \frac{\mu_2 - \mu_1}{\mu_1} a_2 \hat{\eta}, \quad (30)$$

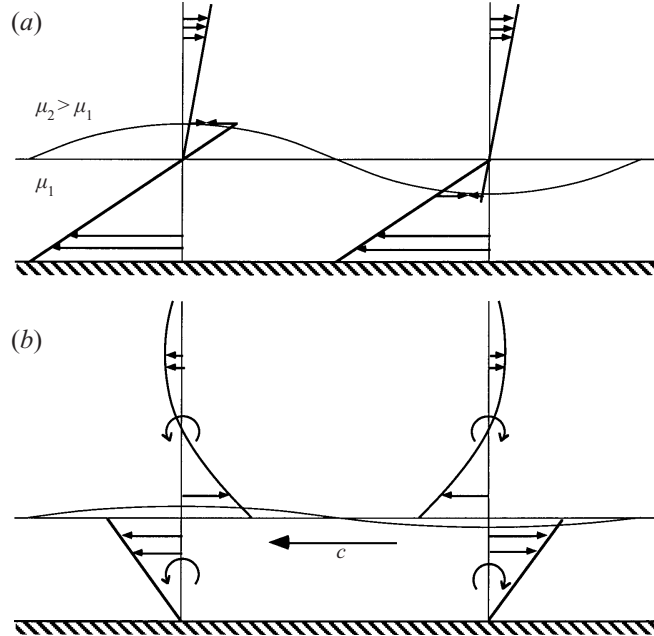


FIGURE 11. (a) Continuity of x -velocity at the deformed interface creates velocity disturbances. (b) Sketch of the profile of the velocity disturbances, and sign of the vorticity disturbances. Mass conservation in the lower fluid imposes wave velocity to the left when $\mu_2 > \mu_1$.

and the velocity field is a combination of a linear shear flow $U(1-y/h_2)$ and a pressure driven flow $-\partial_x \hat{p}_2 y(h_2-y)/2\mu_2$. The pressure gradient is that which is needed to make the total net flow of the two layers equal to zero, i.e. at leading order, that which assures no net flow in the thick layer. Indeed, the flow in the thin layer is $O(h_1^2/h_2^2)$ smaller than that generated by the pressure gradient in the thick layer; thus only a small change in that pressure gradient is needed to make the total net flow of the two layers equal to zero. Hence,

$$\hat{u}_2 = U \left(1 - \frac{y}{h_2} \right) \left(1 - 3 \frac{y}{h_2} \right), \quad (31)$$

with pressure gradient $6\mu_2 U/h_2^2$. This upper layer flow exerts a shear stress $\mu_2 \partial_y \hat{u}_2(0) = -4\mu_2 U/h_2$ on the interface which drives the flow in the thin layer. This flow is then:

$$\hat{u}_1 = -4U \frac{\mu_2/\mu_1}{h_2/h_1} \left(1 + \frac{y}{h_1} \right). \quad (32)$$

Wave propagation is found from mass conservation in the thin layer: the volume $\hat{u}_1(0)h_1\delta t$, leaving the control volume $[0 \leq x \leq \frac{1}{2}\lambda, y < 0]$ during a small time interval δt , must be balanced by a shift of the interface (figure 11b), according to:

$$\hat{u}_1(0)h_1\delta t = \int_0^{\lambda/2} \hat{\eta} [\cos k(x-c\delta t) - \cos kx] dx = 2\hat{\eta} c^{\text{dim}} \delta t, \quad (33)$$

which gives the wave velocity:

$$\frac{c^{\text{dim}}}{a_1 h_1} = 2 \frac{1 - \mu_2/\mu_1}{h_2/h_1}. \quad (34)$$

(Note that the wave velocity may alternatively be obtained from the kinematic condition at the interface, the small vertical flow being calculated from the mass conservation equation.) The results (31) and (32) for the fluid velocity, and (34) for the wave velocity completely agree with Yih's results when the leading terms for $d = h_2/h_1 \gg 1$ are retained, see (A 2) in Appendix C and table 1.

The effects of inertia may be found from either the momentum equations or the vorticity equation. Calculations from the momentum equations are complicated by the vertical advection of the base momentum and by pressure gradients; on the contrary, because the base vorticity is uniform, its advection by the disturbances has no net effect. Thus, the use of the vorticity equation seems preferable; in addition, it allows us to understand how the short-wave mechanism of Hinch (1984) is modified. The leading-order vorticity disturbances,

$$\hat{\omega}_2 = -\partial_y \hat{u}_2 = \frac{U}{h_2} \left(4 - 6 \frac{y}{h_2} \right), \quad (35a)$$

$$\hat{\omega}_1 = -\partial_y \hat{u}_1 = 4 \frac{\mu_2}{\mu_1} \frac{U}{h_2}, \quad (35b)$$

are of same order of magnitude. Since the wave velocity is smaller than the base flow $a_2 h_2$ by $O(h_1^2/h_2^2)$, unsteadiness due to wave propagation can be ignored. Let $\hat{\psi}_2^i$ be the streamfunction of the inertial correction in the thick layer; it is governed by the problem:

$$-\mu_2 \partial_{yyyy} \hat{\psi}_2^i = \rho_2 a_2 y ik \hat{\omega}_2 \quad (36a)$$

with

$$\partial_y \hat{\psi}_2^i = \hat{\psi}_2^i = 0 \quad \text{on } y = 0, \quad y = h_2. \quad (36b)$$

This flow is induced by a torque (the right-hand side of (36a)) acting as if on a viscous fluid (the left-hand side, viscous because inertia is a small correction in the long-wave limit). The zero-velocity condition (36b) comes from the fact that velocity in the thick layer is much larger than in the thin layer, so that, at the leading order, continuity at the interface reduces to the no-slip condition. Integrating, we find:

$$\hat{u}_2^i = \frac{ik \rho_2 a_2 U}{30 h_2^2} y (3y^2 + h_2 y - h_2^2) (h_2 - y)^2. \quad (37)$$

Figure 12 displays the above flow together with the exact eigenfunction, for two values of the viscosity ratio; it turns out that (37) gives a fairly good approximation of the eigenfunction, except in a region of thickness $O(h_1)$ near the interface. For $\mu_2 > \mu_1$ (figure 12a), the positive inertially induced couple in the middle half of the layer creates a positive flow near the interface, whereas the negative inertially induced couple near the upper wall reduces the velocity to zero. For $\mu_2 < \mu_1$ (figure 12b), all velocities are reversed.

In the thin layer, the inertial correction is not driven by the inertia there, but by the shear stress exerted by the inertial correction flow in the thick layer

$$\mu_2 \partial_y \hat{u}_2^i(0) = -i \frac{1}{30} k \rho_2 a_2 U h_2^2,$$

which gives the flow in the thin layer:

$$\hat{u}_1^i = -\frac{ik \rho_2 a_2 U h_2^2}{30 \mu_1} (h_1 + y). \quad (38)$$

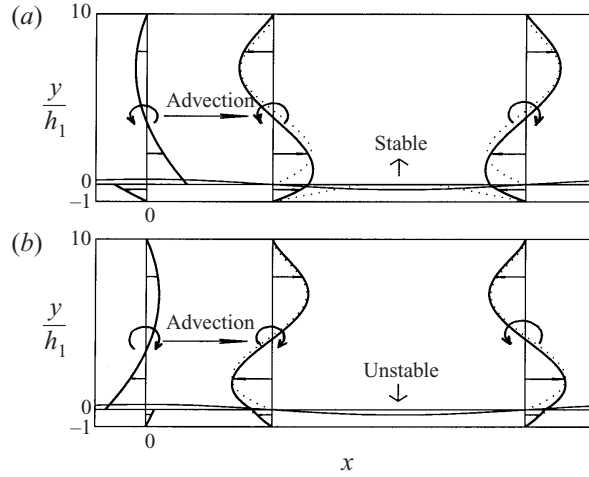


FIGURE 12. Eigenfunctions \hat{u}_j for long waves, for $d = 10, r = 1, Re = 1$. (a) $m = 2$; (b) $m = 0.5$. At $x = 0$: dominant order x -velocity in phase with the interface; at $x = \frac{1}{4}\lambda$ and $x = \frac{3}{4}\lambda$: out-of-phase inertial correction. Dotted lines, equation (37).

Stability (or instability) arises from mass conservation: the volume $\hat{u}_1^i(0)h_1\delta t$, entering (or leaving) the control volume $[\frac{1}{4} \leq x/\lambda \leq \frac{3}{4}, y < 0]$ during a small time interval δt , can be balanced only by a decay (or growth) of the perturbed interface, according to:

$$i\hat{u}_1^i(0)h_1\delta t = \int_{\lambda/4}^{3\lambda/4} \hat{\eta}(e^{\sigma\delta t} - 1) \cos kx \, dx = -\frac{2\hat{\eta}}{k} \sigma^{\text{dim}} \delta t \quad (39)$$

which gives the growth rate:

$$\frac{\sigma^{\text{dim}}}{a_1} = \frac{1 - \mu_2/\mu_1}{60} (kh_1)^2 \frac{\rho_2 a_2 h_2^2}{\mu_2}. \quad (40)$$

Again, the results (37) and (38) for the fluid velocity, and (40) for the growth rate completely agree with Yih's results when the leading terms for $d = h_2/h_1 \gg 1$ are retained, see (A 5) in Appendix C and table 1.

Most of the features of the short-wave mechanism found by Hinch (1984) are present in the long-wave mechanism described above: generation of velocity disturbances in order to satisfy continuity of velocity at the perturbed interface, and advection of the vorticity disturbances by the base flow creating out-of-phase components midway between the peaks and troughs. The important difference for the long waves is the nearness of the lower wall, which reduces everything in the thin layer: the leading-order velocity is reduced there by a factor h_1/h_2 , the out-of-phase vorticity produced by inertia acting there is reduced by h_1^3/h_2^3 , and so the locally induced vertical flow (and so the growth rate) is reduced by h_1^5/h_2^5 . Hence, inertia acts effectively only in the thick layer. Rather subtly, inertia acting in the thick layer does not produce an immediate vertical flow because of the constraint of no net flow. So instead, the thick layer drags the thin layer along with it, which produces a linear flow within the thin layer, and it is the horizontal divergence of this flow which causes growth. Hence, the growth depends on the sign of the flow in the thick layer, which depends on whether the thin or thick layer is the less viscous.

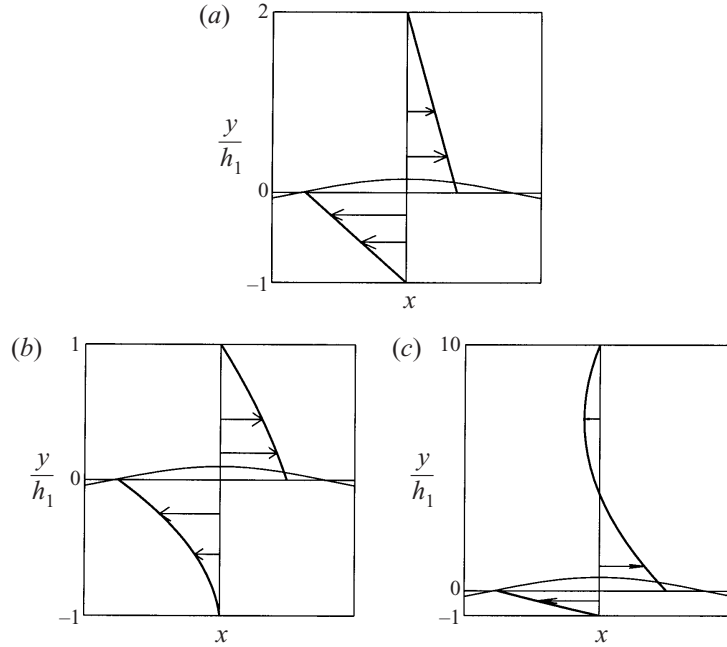


FIGURE 13. Dominant order x -velocity $\hat{u}_j^{(0)}$ for $m = 4$. (a) $d^2 = 4 = m$; (b) $d^2 = 1 < m$; (c) $d^2 = 100 > m$.

4.2. Channel flow: case of layers with similar thickness ($\alpha_1 \approx \alpha_2 \ll 1$)

As mentioned in the previous section, pressure disturbances develop in order to satisfy the requirement (28) of no net disturbance flow. However, linear profiles fulfil this requirement, i.e. verify $h_1 \hat{u}_1(0) = -h_2 \hat{u}_2(0)$, and also satisfy continuity of shear stress if $(h_2/h_1)^2 = \mu_2/\mu_1$. Hence, the presence of the factor $(d^2 - m)$ in the pressure disturbance (see Appendix C). Thus, when viscosities and layer thicknesses are such that $d^2 \approx m$, the pressure disturbance plays a negligible role and velocity profiles are linear in both fluids (figure 13a):

$$\hat{u}_1 = -U \frac{\mu_2/\mu_1}{h_2/h_1} (1 + y/h_1), \quad \hat{u}_2 = U(1 - y/h_2), \quad (41)$$

with

$$U := \hat{u}_2(0) = \frac{\mu_2 - \mu_1}{\mu_2} \frac{h_2/h_1}{\mu_2/\mu_1 + h_2/h_1} a_1 \hat{\eta}.$$

Otherwise, the pressure disturbance induces negative velocity curvature when $d^2 < m$ (figure 13b) or positive curvature when $d^2 > m$ (figure 13c), with negligible curvature effects in the lower fluid when $d \gg 1$. The wave velocity can be calculated from mass conservation as in the previous subsection, leading to:

$$\frac{c^{\text{dim}}}{a_1 h_1} = \frac{1}{2} \frac{1 - \mu_2/\mu_1}{\mu_2/\mu_1 + h_2/h_1}. \quad (42)$$

When $d^2 = m$, (41) and (42) are exactly Yih's results; when $d^2 \approx m \approx 1$, i.e. for layers with nearly equal thickness and viscosity, (41) and (42) corresponds to (A 3) in Appendix C and to the wave velocity given in table 1.

Inertial effects may be taken into account as previously. However, the velocities

have the same order of magnitude in both fluids, and the momentum (or vorticity) equations cannot be uncoupled, leading to less simple calculations. A simple estimate of the growth rate may be obtained when $d^2 \approx m \approx 1$ as follows. For nearly equal viscosities, the wave velocity is small, and unsteadiness can be neglected in the inertia terms. First, consider the case $\rho_1 = 0$, i.e. the lower fluid with negligible inertia; figure 14(a) displays the corresponding eigenfunctions for long waves. In the upper layer, advection of the vorticity disturbances $\hat{\omega}_2 \approx U/h_2$ creates an out-of-phase component $\hat{\omega}_2^i \sim -iRe_{eff2}\hat{\omega}_2$, where $Re_{eff2} := \alpha_2^3/\beta_2^3 = (kh_2)(\rho_2 a_2 h_2^2/\mu_2)$ is the effective Reynolds number defined in §3. This out-of-phase vorticity corresponds to velocity $\hat{u}_2^i \sim \hat{\omega}_2^i h_2 \sim -iRe_{eff2}U$. In order to satisfy the no net flow condition, a counter-flow $\hat{u}_1^i \sim -\hat{u}_2^i$ must develop in the lower layer, which is created by the pressure gradient $ik\hat{p}_1^i \sim \mu_1(-\hat{u}_1^i/h_1^2)$, i.e. by the pressure $\hat{p}_1^i \sim -\rho_2 a_2 h_2 U$. Since $\hat{p}_2^i = \hat{p}_1^i$, this pressure modifies slightly the flow in the upper layer but does not change the magnitude of the velocity there. This out-of-phase flow gives rise to amplification or decay of the interfacial disturbance according to the mass conservation equation (39), leading to the growth rate:

$$\sigma^{\text{dim}} = ikh_1 \frac{\hat{u}_1^i(0)}{\hat{\eta}} = a_1(1 - \mu_2/\mu_1)(kh_1)^2 \frac{\rho_1 a_1 h_1^2}{\mu_1}.$$

Figure 14(b) displays the eigenfunctions when $\rho_1/\rho_2 = 0.5$, and shows that the above reasoning for $\rho_1 = 0$ holds as long as $\rho_1 < \rho_2$, with flows dominated by inertia in the upper fluid and by the pressure gradient in the lower fluid. Consider now the opposite case $\rho_2 = 0$ (figure 15a); a similar reasoning shows that (i) the flow in layer 1 is driven by inertia with velocity $\hat{u}_1^i \sim iRe_{eff1}U$, and (ii) the flow in layer 2 is driven by the pressure $\hat{p}_2^i \sim -\rho_1 a_1 h_1 U$, leading to growth rate $\sigma^{\text{dim}}/a_1 = (1 - \mu_2/\mu_1)(kh_1)^2(\rho_1 a_1 h_1^2/\mu_1)$. Figure 15(b) displays the eigenfunctions when $\rho_1/\rho_2 = 2$, and shows that the reasoning for $\rho_2 = 0$ holds as long as $\rho_2 < \rho_1$. Finally, for fluids with similar inertia, the resulting flow can be considered as the superposition of the above two flows, leading to the following pressure disturbance and growth rate:

$$\hat{p}_1^i = \hat{p}_2^i \sim \left(1 - \frac{\mu_2}{\mu_1}\right) (\rho_1 + \rho_2) a_1^2 h_1 \hat{\eta} \quad (43)$$

$$\frac{\sigma^{\text{dim}}}{a_1} = (kh_1)^2 \left(1 - \frac{\mu_2}{\mu_1}\right) \left(1 - \frac{\rho_2}{\rho_1}\right) \frac{\rho_1 a_1 h_1^2}{\mu_1}. \quad (44)$$

The pressure (43) and growth rate (44) agree with the long-wave results, giving the right dependence with all parameters, see (A 6) in Appendix C and table 1.

4.3. Semi-bounded flow ($\alpha_1 \ll 1$ and $\alpha_2 \gg 1$)

When the upper wall is at a distance from the interface greater than the wavelength, it plays no more role, the vertical gradients in the upper fluid are no longer of order $1/h_2$, and the analysis performed in §4.1 must be slightly modified. Rather than following exactly the same approach as in §4.1, we use in this section the results obtained in §3 on the penetration depth δ_j and the effective Reynolds number Re_{effj} to derive estimates of the wave velocity and growth rate.

The lower layer is assumed to be in the shallow viscous regime ($\alpha_1 \ll 1$ and $\alpha_1 \ll \beta_1$), with dimensional penetration depth $\delta_1^{\text{dim}} = \delta_1/k \sim h_1$ and effective Reynolds number $Re_{eff1} \sim \alpha_1 Re$; the upper layer is assumed to be in the inviscid regime ($\alpha_2 \gg \beta_2$ and $\beta_2 \ll 1$), with dimensional penetration depth $\delta_2^{\text{dim}} = \delta_2/k \sim \beta_2/k$ and effective Reynolds number $Re_{eff2} \sim 1$. Since $\beta_1 \sim \beta_2$ for fluids with similar viscosity and

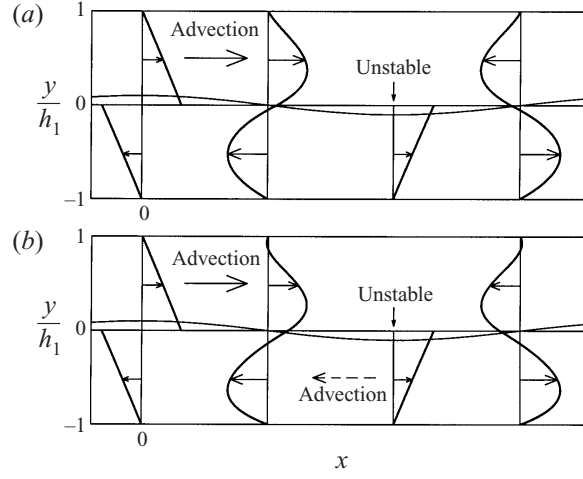


FIGURE 14. Eigenfunctions \hat{u}_j for long waves, for $d = 1, m = 1.1, Re = 1$. (a) $\rho_1 = 0$; (b) $\rho_1 = 0.5\rho_2$. At $x = 0$ and $x = \frac{1}{2}\lambda$: dominant order x -velocity in phase with the interface; at $x = \frac{1}{4}\lambda$ and $x = \frac{3}{4}\lambda$: out-of-phase inertial correction.

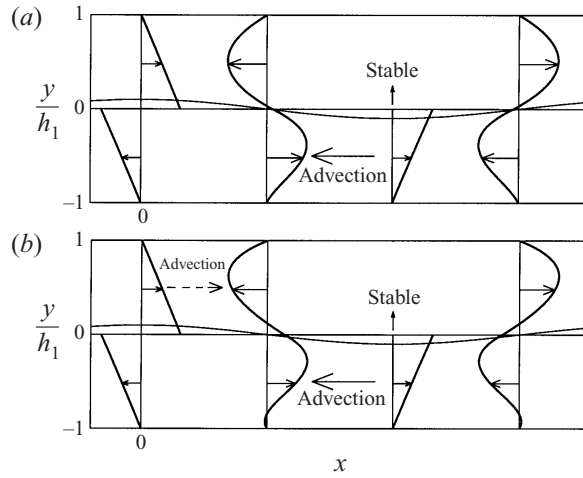


FIGURE 15. Eigenfunctions \hat{u}_j for long waves, for $d = 1, m = 1.1, Re = 1$. (a) $\rho_2 = 0$; (b) $\rho_2 = 0.5\rho_1$. At $x = 0$ and $x = \frac{1}{2}\lambda$: dominant order x -velocity in phase with the interface; at $x = \frac{1}{4}\lambda$ and $x = \frac{3}{4}\lambda$: out-of-phase inertial correction.

density, we have $\delta_1^{\text{dim}} \ll \delta_2^{\text{dim}}$, with:

$$\frac{\delta_1^{\text{dim}}}{\delta_2^{\text{dim}}} \sim \frac{h_1}{(k^2 \mu_2 / \rho_2 a_2)^{1/3} / k} = (kh_1)^{1/3} \left(\frac{rRe}{m^2} \right)^{1/3}. \quad (45)$$

Thus, continuity of shear stress at the interface,

$$\mu_1 \frac{\hat{u}_1(0)}{\delta_1^{\text{dim}}} \sim \mu_2 \frac{-\hat{u}_2(0)}{\delta_2^{\text{dim}}},$$

implies that \hat{u}_1 is much smaller than \hat{u}_2 . Then continuity of x -velocity (27) gives:

$$U := \hat{u}_2(0) \sim \frac{\mu_2 - \mu_1}{\mu_2} a_1 \hat{\eta}.$$

Hence, in the thin layer, the linear shear flow in phase with the interface is such that:

$$\hat{u}_1(0) \sim -\frac{\delta_1^{\text{dim}}}{\delta_2^{\text{dim}}} \frac{\mu_2 - \mu_1}{\mu_1} a_1 \hat{\eta},$$

which, together with mass conservation (33), gives the wave velocity:

$$\frac{c^{\text{dim}}}{a_1 h_1} \sim \frac{\delta_1^{\text{dim}}}{\delta_2^{\text{dim}}} \frac{\mu_1 - \mu_2}{\mu_1}. \quad (46)$$

Together with (45), (46) is exactly the wave velocity obtained by Hooper (1985), except for the numerical factor 0.46 (see table 2). Note that, unlike the case of channel flow, waves are dispersive, because the penetration depth in the thick layer depends on the wavelength.

Advection of the vorticity disturbances $\hat{\omega}_2 \sim U/\delta_2^{\text{dim}}$ by the base flow in the upper fluid creates an out-of-phase vorticity component $\hat{\omega}_2^i \sim -i Re_{eff2} \hat{\omega}_2$, which induces a shear stress $\mu_2 \hat{\omega}_2^i$ on the lower fluid. This shear stress creates in turn a linear flow in the thin layer such that $\hat{u}_1^i(0) \sim \mu_2/\mu_1 h_1 \hat{\omega}_2^i$, which, together with mass conservation (33), gives the growth rate σ :

$$\frac{\sigma^{\text{dim}}}{a_1} = \frac{-i \hat{u}_1^i(0) k h_1}{2 a_1 \hat{\eta}} \sim k h_1 \frac{\mu_1 - \mu_2}{\mu_1} \frac{\delta_1^{\text{dim}}}{\delta_2^{\text{dim}}} Re_{eff2}. \quad (47)$$

With $Re_{eff2} = 1$ and $\delta_1^{\text{dim}}/\delta_2^{\text{dim}}$ given by (45), this is exactly the growth rate obtained by Hooper (1985) for semi-bounded flows, except for the numerical factor (see table 2). Note that the reasoning leading to (47) holds for channel flows with $Re_{eff2} = (k h_2)(\rho_2 a_2 h_2^2/\mu_2)$ and $\delta_1^{\text{dim}}/\delta_2^{\text{dim}} = h_1/h_2$, giving (40) back. Finally, the mechanism for the long-wave instability for semi-bounded flows is the same as for channel flows, the difference in the growth rate arising from the difference in the penetration depth and effective Reynolds number in the thick layer.

5. Summary and conclusion

In order to gain better physical insight into the numerous linear stability results for the two-layer Couette flow, we have first considered the much simpler problem of the single-fluid Couette flow over a wavy solid boundary. Taking the inverse wavenumber as the unit length, this problem depends on two parameters only: the dimensionless thickness α and a diffusion length β . Three different flow regimes have been exhibited: the shallow viscous, the deep viscous, and the inviscid regimes. Each regime occupies a well-defined region in the (β, α) -plane, defining a ‘phase diagram’, and is characterized by a penetration depth δ of vorticity disturbances, and an effective Reynolds number Re_{eff} measuring the importance of inertial effects on disturbances (figure 6).

Then, armed with the idea of the phase diagram, we came back to the two-layer Couette flow. Ignoring gravity and surface tension, this problem depends on four parameters: two dimensionless thicknesses α_j and two viscous lengths β_j . Analysing the eigenfunctions from the existing literature, it appears that on considering the penetration depth δ_j of vorticity disturbances induced by the slightly deformed interface, as well as the effective Reynolds number Re_{effj} , several flow regimes can be

defined. Remarkably, these flow regimes are the same as those of the single-fluid flow, with the same scalings for the penetration depth and the effective Reynolds number, allowing the construction of phase diagrams of the flow regimes, one for channel flows and one for semi-bounded flows. Then, each type of instability is associated with one flow regime: the long-wave instability found by Yih (1967) is typical of the shallow viscous regime, and the short-wave instability found by Hooper & Boyd (1983) is typical of the deep viscous regime. No interfacial instability arises in the inviscid regime. However, in the latter regime, which corresponds to strong shear rates, a wall mode of instability may appear (Hooper & Boyd 1987). Analysis of the available numerical results confirms the relevance of the phase diagram (figure 8). Moreover, it appears that the domain of existence of an instability extends beyond the validity domain of the asymptotic expansion by which it was primarily discovered. For instance, the long-wave instability is typical of all situations when the walls bound the diffusion of vorticity, i.e. when the wavelength and viscous lengths are greater than the layer thicknesses. Similarly, the short-wave instability typically arises for wavelengths smaller than the layer thicknesses and viscous lengths. Finally, on considering the lines of constant shear Reynolds number in the phase diagram (figure 9), each wavenumber appears to fall into a particular flow regime, and typical curves giving the growth rate versus wavenumber can be depicted (figure 10).

The basis of this unified view of interfacial instabilities is the comparison between the three lengthscales involved in each fluid layer, namely the wavelength, the layer thickness and the diffusion length: the penetration depth of vorticity disturbances must scale with one of these lengths, leading to the three flow regimes (when fluid properties are assumed to be of the same order of magnitude). This picture is significantly different and simpler than that proposed by Hooper & Boyd (1987), who found four regimes (their regime (iv) must be merged partly with their regime (i), and form the deep viscous regime, and partly with their regime (ii), and form the shallow viscous regime).

The second part of this paper was devoted to the mechanism for the long-wave instability, and to an explanation of the 'thin-layer effect'. As for the short-wave instability, the initiating mechanism is that the base velocities do not match on the disturbed interface, and velocity disturbances must develop in order to satisfy continuity: this instability is a 'velocity-induced instability', as opposed to the 'stress-induced instability' typical of free-falling films (Smith 1990). Three typical situations have been studied: (i) channel flow with a thin layer, (ii) channel flow with nearly equal layer thickness, and (iii) semi-bounded flow over a thin layer. For all cases, the requirement of no net flow for the disturbances creates a pressure gradient, and, because of the presence of the wall, mass conservation in each fluid implies a shift of the interface with the less viscous fluid, which corresponds to the wave velocity. In each case, good estimates have been obtained for the wave velocity and the dominant Stokes flow of the disturbances.

Instability then arises from small inertial effects. For a thin layer, inertial effects in the thick layer are much greater than in the thin layer, and create an out-of-phase flow which exerts a shear stress on the thin layer; this shear stress drives a small out-of-phase flow in the thin layer which is responsible for the growth or decay of the initial interfacial disturbance. The sign of the viscosity difference imposes the sign of the velocity disturbances, which impose in turn the sign of the growth rate, which originates the 'thin-layer effect'. Moreover, the growth rate appears to be proportional to the ratio δ_1/δ_2 of the penetration depths, which explains why it scales as k^2 for channel flow and as $k^{4/3}$ for semi-bounded flow. For layers with nearly equal thickness

and viscosity, inertial effects have the same order of magnitude in both fluids and compete with one another; the sign of the out-of-phase flow is imposed by the heavier fluid which has more inertia, whereas a pressure gradient develops in order to reverse the disturbance flow in the lighter fluid and satisfy the requirement of no net flow. In all cases, simple estimates give the right dependence of the growth rate against all parameters.

Finally, the ‘thin-layer effect’ is typical of multi-layer flows, such as pressure-driven plane or annular flows, or gravity-driven flows down an inclined plane. The jump in the slope of the basic state owing to the viscosity difference generally plays a central role in originating the disturbance flow, but may not be necessary. For instance, for the vertical core-annular Poiseuille flow with equal viscosity, the disturbance flow arises from the jump in the curvature of the basic state owing to density difference (Smith 1989).

Appendix A. Constants C_j in (6) and (7) for the single-fluid Couette flow

$$C_1 = \frac{B^+ - B^-}{A^+B^- - A^-B^+}, \quad C_2 = -\frac{A^+ - A^-}{A^+B^- - A^-B^+}, \quad C_3 = \frac{1}{2}, \quad C_4 = 0,$$

with

$$A^\pm = \int_0^\alpha e^{\pm y} \text{Ai}(z(y)) dy, \quad B^\pm = \int_0^\alpha e^{\pm y} \text{Bi}(z(y)) dy,$$

and

$$z(y) = \frac{1}{\beta}(y - i\beta^3)e^{i\pi/6}.$$

Appendix B. Wave velocity and growth rate of wall modes (Hooper & Boyd 1987)

For $\beta_1/\alpha_1 \ll 1$, $\beta_1 \ll 1$ and $r = 1$, for channel flows:

$$c^{\text{dim}} \sim \frac{a_1}{k} C, \quad C = \frac{1 - m \sinh \alpha_1 \sinh \alpha_2}{m \sinh(\alpha_1 + \alpha_2)}$$

$$\frac{\sigma^{\text{dim}}}{a_1} \sim -k \left(\frac{v_1}{a_1} \right)^{1/2} \frac{(\alpha_1 + C)^{-1/2} \sinh^2 \alpha_2 - m(\alpha_2 - mC)^{-1/2} \sinh^2 \alpha_1}{2^{1/2} \sinh^2(\alpha_1 + \alpha_2)}$$

and for semi-bounded flows:

$$c^{\text{dim}} \sim \frac{a_1}{k} C, \quad C = \frac{1 - m}{2m} (1 - \exp(-2\alpha_1))$$

$$\frac{\sigma^{\text{dim}}}{a_1} \sim -k \left(\frac{v_1}{a_1} \right)^{1/2} \frac{1 - m}{m} \frac{\exp(-2\alpha_1)}{2^{1/2}(\alpha_1 + C)^{1/2}}.$$

Appendix C. Long-wave instability results

We recall here the solution of the conservation equations (19) and boundary conditions (20) obtained by Yih (1967) for Couette flow, with $\alpha_1 \ll 1$ and $Re = \alpha_1^2/\beta_1^3 = O(1)$. In addition to the results for the velocity and pressure eigenfunctions, simpler results are also given for (i) a thin lower layer ($d \gg 1$), and (ii) layers with

close thickness and viscosity ($d \approx 1, m \approx 1$). We choose the normalization condition $\hat{\eta} = k\hat{\eta}^{\text{dim}} = 1$. In order to rescale transverse gradients ∂_y to $O(1)$, we introduce $Y = y/\alpha_1$. Expanding the velocities and pressure in powers of α_1 , (19) and (20) give, at the leading order:

$$i\hat{u}_j^{(0)} + \partial_Y \hat{v}_j^{(1)} = 0 \quad (j = 1, 2),$$

$$0 = -i\hat{p}_j^{(0)} + \frac{m_j}{Re} \partial_{YY} \hat{u}_j^{(0)} \quad (j = 1, 2),$$

$$0 = \partial_Y \hat{p}_j^{(0)} \quad (j = 1, 2),$$

with the boundary conditions at the walls $Y = -1$ and $Y = d$:

$$\hat{u}_1^{(0)}(-1) = 0, \quad \hat{v}_1^{(1)}(-1) = 0,$$

$$\hat{u}_2^{(0)}(d) = 0, \quad \hat{v}_2^{(1)}(d) = 0,$$

and the boundary conditions at the interface $Y = 0$:

$$1 + \hat{u}_1^{(0)} = \frac{1}{m} + \hat{u}_2^{(0)}, \quad \hat{v}_1^{(1)} = \hat{v}_2^{(1)},$$

$$\partial_Y \hat{u}_1^{(0)} = m\partial_Y \hat{u}_2^{(0)}, \quad \hat{p}_2^{(0)} = \hat{p}_1^{(0)},$$

$$-ic^{(1)} - \hat{v}_j^{(1)} = 0.$$

The general solution satisfying the conservation equations, the no-slip conditions at the walls and continuity of normal stress at the interface is given by:

$$\hat{u}_1^{(0)} = (Y + 1) \left(-\frac{Re p_0}{2} Y + \hat{u}_1^{(0)}(0) \right), \quad \hat{v}_1^{(1)} = -i \int_{-1}^Y \hat{u}_1^{(0)} dy, \quad (\text{C } 1a)$$

$$\hat{u}_2^{(0)} = \left(\frac{Y}{d} - 1 \right) \left(-\frac{Re p_0 d}{2m} Y - \hat{u}_2^{(0)}(0) \right), \quad \hat{v}_2^{(1)} = -i \int_d^Y \hat{u}_2^{(0)} dy. \quad (\text{C } 1b)$$

Continuity of tangential stress and velocity at the interface then gives:

$$\hat{p}_2^{(0)} = \hat{p}_1^{(0)} = ip_0 = \frac{i}{Re} \frac{6(1-m)(d^2 - m)}{D(m, d)},$$

$$\hat{u}_1^{(0)}(0) = \frac{1-m}{D(m, d)} (m + 3d^2 + 4d^3),$$

$$\hat{u}_2^{(0)}(0) = \frac{(1-m)d}{mD(m, d)} (4m + 3md + d^3),$$

$$c^{(1)} = i\hat{v}_j^{(1)}(0) = \frac{2(1-m)d^2(1+d)}{D(m, d)},$$

$$D(m, d) = d^4 + 4dm + 6d^2m + 4d^3m + m^2.$$

At this order, the eigenvalue $c^{(1)}$ is real and corresponds to the dimensional wave velocity $c^{\text{dim}} = \alpha_1 c^{(1)} a_1 / k = a_1 h_1 c^{(1)}$. Note that non-zero wave velocity is consistent with the reversibility of the Stokes flow described by these leading-order equations: reversing the base flow velocity simply reverses the wave velocity.

For a thin lower layer ($d \gg 1$), the wave velocity is given in table 1, and the above

expressions for the pressure and fluid velocity give:

$$\left. \begin{aligned} \hat{p}_2^{(0)} &= \hat{p}_1^{(0)} \approx -i \frac{6}{Re} \frac{1-m}{d^2}, \\ \hat{u}_1^{(0)} &= \frac{4(1-m)}{d}(Y+1), \\ \hat{u}_2^{(0)} &= \frac{1-m}{m} \left(\frac{Y}{d} - 1 \right) \left(-3 \frac{Y}{d} + 1 \right). \end{aligned} \right\} \quad (C2)$$

For nearly equal viscosity ($|1-m| \ll 1$) and layer thickness ($|1-d| \ll 1$), the wave velocity is given in table 1, and the pressure and fluid velocity simplify to give:

$$\left. \begin{aligned} \hat{p}_2^{(0)} &= \hat{p}_1^{(0)} \approx -i \frac{3}{4Re} (1-m)(1-d), \\ \hat{u}_1^{(0)} &\approx \frac{1-m}{2}(Y+1), \\ \hat{u}_2^{(0)} &\approx \frac{1-m}{2}(Y-d). \end{aligned} \right\} \quad (C3)$$

In both fluids, the pressure disturbance is very small, and the motion is essentially a shear flow driven by the shear stress disturbance at the interface.

At the next order in the perturbation expansion, the equations to be solved are:

$$\begin{aligned} i\hat{u}_j^{(1)} + \partial_Y \hat{v}_j^{(2)} &= 0 \quad (j = 1, 2), \\ r_j \{ i(Y/m_j - c^{(1)})\hat{u}_j^{(0)} + \hat{v}_j^{(1)}/m_j \} &= -i\hat{p}_j^{(1)} + \frac{m_j}{Re} \partial_{YY} \hat{u}_j^{(1)} \quad (j = 1, 2), \\ 0 &= \partial_Y \hat{p}_j^{(1)} \quad (j = 1, 2), \end{aligned}$$

with the boundary conditions at the walls $Y = -1$ and $Y = d$:

$$\begin{aligned} \hat{u}_1^{(1)}(-1) &= 0, \quad \hat{v}_1^{(2)}(-1) = 0, \\ \hat{u}_2^{(1)}(d) &= 0, \quad \hat{v}_2^{(2)}(d) = 0, \end{aligned}$$

and the boundary conditions at the interface $Y = 0$:

$$\begin{aligned} \hat{u}_1^{(1)} &= \hat{u}_2^{(1)}, \quad \hat{v}_1^{(2)} = \hat{v}_2^{(2)}, \\ \partial_Y \hat{u}_1^{(1)} &= m \partial_Y \hat{u}_2^{(1)}, \quad -\hat{p}_2^{(1)} + \hat{p}_1^{(1)} = 0, \\ -ic^{(2)} - \hat{v}_j^{(2)} &= 0. \end{aligned}$$

The solution of these equations is obtained as for the zeroth-order and gives:

$$\hat{u}_1^{(1)} = iRe \int_{-1}^Y dY \left(\int_{-1}^Y (p_1 + (Y - c^{(1)})\hat{u}_1^{(0)} - i\hat{v}_1^{(1)}) dY + \tau_{\text{int}} \right), \quad (C4a)$$

$$\hat{u}_2^{(1)} = \frac{iRe}{m} \int_d^Y dY \left(\int_d^Y (p_1 + r(Y/m - c^{(1)})\hat{u}_2^{(0)} - ir/m \hat{v}_2^{(1)}) dY + \tau_{\text{int}} \right), \quad (C4b)$$

with:

$$\begin{aligned}
 p_1 = & \frac{(-1+m)}{5m^2 D(m,d)^3} (-25d^9 m^3 - m^3(20m+139)d^8 - 2m^3(69m+145)d^7 \\
 & - m^3(271+349m+8m^2)d^6 - 3m^3(15m^2+131m+32)d^5 - 10m^4(8m+17)d^4 \\
 & - 4m^4(9m+m^2+1)d^3 - m^5(m-13)d^2 + 7m^6 d + m^7 \\
 & + r(d^{13} + 7d^{12}m + m(-1+13m)d^{11} - 4m(9m+m^2+1)d^{10} - 10m^2(17m+8)d^9 \\
 & - 3m^2(32m^2+15+131m)d^8 - m^2(271m^2+349m+8)d^7 - 2m^3(69+145m)d^6 \\
 & - m^3(20+139m)d^5 - 25m^4 d^4),
 \end{aligned}$$

$$\begin{aligned}
 \tau_{\text{int}} = & \frac{(1-m)}{30m^2 D(m,d)^3} (-100d^{10} m^3 - 4m^3(131+20m)d^9 - m^3(1025+496m)d^8 \\
 & - 24m^3(48m+37)d^7 - 4m^3(72+11m^2+298m)d^6 - 4m^4(23m+121)d^5 \\
 & - 6m^4(5m+4)d^4 + 8m^5(2+m)d^3 + 8m^5(-1+m)d^2 \\
 & - 4m^6 d - m^7 + r(d^{14} + 4d^{13}m + 8m(-1+m)d^{12} - 8m(1+2m)d^{11} \\
 & + 6m^2(4m+5)d^{10} + 4m^2(121m+23)d^9 + 4m^2(72m^2+298m+11)d^8 \\
 & + 24m^3(37m+48)d^7 + m^3(496+1025m)d^6 + 4m^3(131m+20)d^5 + 100m^4 d^4),
 \end{aligned}$$

$$\begin{aligned}
 -ic^{(2)} = \hat{v}_1^{(2)}(0) = \hat{v}_2^{(2)}(0) = & \frac{Re(1-m)d^2}{60m^2 D(m,d)^3} (32d^9 m^2 + m^2(56m+135)d^8 \\
 & + 4m^2(8m^2+61m+49)d^7 + 4m^2(34m^2+95m+24)d^6 + 4m^3(57m+49)d^5 \\
 & + 2m^3(8m^2+57m-4)d^4 + 12m^4(m-3)d^3 - 4m^4(2+5m)d^2 \\
 & - 4m^5(m+1)d - m^6 + r(d^{12} + 4(m+1)d^{11} + 4m(2m+5)d^{10} + 12m(3m-1)d^9 \\
 & + 2m(4m^2-57m-8)d^8 - 4m^2(49m+57)d^7 - 4m^2(24m^2+95m+34)d^6 \\
 & - 4m^2(49m^2+61m+8)d^5 - m^3(135m+56)d^4 - 32m^4 d^3).
 \end{aligned}$$

At this order, the eigenvalue $c^{(2)}$ is imaginary and corresponds to the dimensional growth rate $\sigma^{\text{dim}} = -i\alpha_1^2 c^{(2)} a_1$.

For a thin lower layer ($d \gg 1$), the growth rate is given in table 1, and the pressure and fluid velocities are:

$$\left. \begin{aligned}
 \hat{p}_2^{(1)} = \hat{p}_1^{(1)} = p_1 & \approx -\frac{1}{5} \frac{r(1-m)}{m^2} d, \\
 \hat{u}_1^{(1)} & \approx iRe \frac{r(1-m)d^2}{30m^2} \{Y+1\}, \\
 \hat{u}_2^{(1)} & \approx iRe \frac{r(1-m)d^2}{30m^2} \left\{ dQ_1 \left(\frac{Y}{d} \right) + d^0 Q_0 \left(\frac{Y}{d} \right) + d^{-1} Q_{-1} \left(\frac{Y}{d} \right) + O(d^{-2}) \right\},
 \end{aligned} \right\} \quad (C5)$$

where the Q_j are polynomials given by:

$$Q_1(y) = \frac{1}{m}y(y-1)^2(-3y^2 - y + 1),$$

$$Q_0(y) = (y-1)(12y^4 - 8y^3 - 8y^2 + 7y - 1),$$

$$Q_{-1}(y) = (y-1)(21y^4 + 6y^3 - 34y^2 + 23y - 3 - m(48y^4 - 17y^3 - 57y^2 + 48y - 8)).$$

In the upper layer, the leading Q_1 -term gives the right behaviour far from the interface, the Q_0 -term gives the right behaviour near the interface and matches the velocities at the interface ($Q_1(0) = 0$ and $Q_0(0) = 1$). However, the net flux arising from each of these terms is zero. The dominant mass flux is obtained from the Q_{-1} -term, which gives the growth rate shown in table 1.

For nearly equal viscosities ($|1 - m| \ll 1$) and layer thicknesses ($|1 - d| \ll 1$), the growth rate is given in table 1, and pressure and fluid velocity are:

$$\hat{p}_2^{(1)} = \hat{p}_1^{(1)} = p_1 \approx (1 - m)\frac{1 + r}{10},$$

$$\hat{u}_1^{(1)} \approx iRe\frac{1 - m}{480}Q_0(Y, r), \quad (C 6)$$

$$\hat{u}_2^{(1)} \approx iRe\frac{1 - m}{480}rQ_0(-Y, 1/r),$$

where

$$Q_0(Y, r) = (Y + 1)(10Y^3 - 10Y^2 - 26Y + 1 + r(24Y + 1)).$$

REFERENCES

- ALBERT, F. & CHARRU, F. 2000 Small Reynolds number instabilities in two-layer Couette flow. *Eur. J. Mech.* **19**, 229–252.
- BARTHELET, P., CHARRU, F. & FABRE, J. 1995 Experimental study of interfacial long waves in a two-layer shear flow. *J. Fluid Mech.* **303**, 23–53.
- BATCHELOR, G. K. 1967 *An Introduction to Fluid Dynamics*. Cambridge University Press.
- CHARRU, F. & BARTHELET, P. 1999 Secondary instabilities of interfacial waves due to coupling with a long wave mode in a two-layer Couette flow. *Physica D* **125**, 311–324.
- GOUSSIS, D. A. & KELLY, R. E. 1988 Mechanisms and conditions for an instability of shear flow in the presence of an interface. *Unpublished*.
- HESLA, T. I., PRANCKH, F. R. & PREZIOSI, L. 1986 Squire's theorem for two stratified fluids. *Phys. Fluids* **29**, 2808–2811.
- HINCH, E. J. 1984 A note on the mechanism of the instability at the interface between two shearing fluids. *J. Fluid Mech.* **144**, 463–465.
- HOOPER, A. P. 1985 Long-wave instability at the interface between two viscous fluids: thin layer effects. *Phys. Fluids* **28**, 1613–1618.
- HOOPER, A. P. 1989 The stability of two superposed viscous fluids in a channel. *Phys. Fluids A* **1**, 1133–1142.
- HOOPER, A. P. & BOYD, W. G. C. 1983 Shear-flow instability at the interface between two viscous fluids. *J. Fluid Mech.* **128**, 507–528.
- HOOPER, A. P. & BOYD, W. G. C. 1987 Shear flow instability due to a wall and a viscosity difference at the interface. *J. Fluid Mech.* **179**, 201–225.
- JOSEPH, D. D., BAI, R., CHEN, K. P. & RENARDY, Y. 1997 Core-annular flows. *Ann. Rev. Fluid Mech.* **29**, 65–90.
- KLIAKHANDLER, I. L. & SIVASHINSKY, G. I. 1997 Viscous damping and instabilities in stratified liquid film flowing down a slightly inclined plane. *Phys. Fluids* **9**, 23–30.

- LAURE, P., LE MEUR, H., DEMAY, Y., SAUT, J. C. & SCOTTO, S. 1997 Linear stability of multilayer plane Poiseuille flows of Oldroyd-B fluid. *J. Non-Newtonian Fluid Mech.* **71**, 1–23.
- RENARDY, Y. 1985 Instability at the interface between two shearing fluids in a channel. *Phys. Fluids* **28**, 3441–3443.
- RENARDY, Y. 1987 The thin layer effect and interfacial stability in a two-layer Couette flow with similar liquids. *Phys. Fluids* **30**, 1627–1637.
- SANGALLI, M., GALLAGHER, C. T., LEIGHTON, D. T., CHANG, H.-C. & MCCREADY, M. J. 1995 Finite-amplitude waves at the interface between fluids with different viscosity: theory and experiments. *Phys. Rev. Lett.* **75**, 77–80.
- SMITH, M. K. 1989 The axisymmetric long-wave instability of a concentric two-phase pipe flow. *Phys. Fluids A* **1**, 494–506.
- SMITH, M. K. 1990 The mechanism for the long-wave instability in thin liquid films. *J. Fluid Mech.* **217**, 469–485.
- WANG, C. K., SEABORG, J. J. & LIN, S. P. 1978 Instability of multi-layered liquid films. *Phys. Fluids* **21**, 1669–1673.
- YIH, C. S. 1967 Instability due to viscous stratification. *J. Fluid Mech.* **27**, 337–352.